Liquid Crystals
Publication details, including instructions for authors and subscription information:
http://www.informaworld.com/smpp/title~content=t713926090

Non-equilibrium molecular-dynamics measurement of the Leslie coefficients of a Gay-Berne nematic liquid crystal

Congmin Wu[a]; Tiezheng Qian[b]; Pingwen Zhang[a]
[a] LMAM, CCSE and School of Mathematical Science, Peking University, Beijing 100871, China [b] Department of Mathematics, The Hong Kong University of Science and Technology, Kowloon, Hong Kong, China

To cite this Article Wu, Congmin , Qian, Tiezheng and Zhang, Pingwen(2007) 'Non-equilibrium molecular-dynamics measurement of the Leslie coefficients of a Gay-Berne nematic liquid crystal', Liquid Crystals, 34: 10, 1175 — 1184
To link to this Article: DOI: 10.1080/02678290701663878
URL: http://dx.doi.org/10.1080/02678290701663878

Liquid Crystals, Vol. 34, No. 10, October 2007, 1175–1184

Non-equilibrium molecular-dynamics measurement of the Leslie coefficients of a Gay–Berne nematic liquid crystal

CONGMIN WU†, TIEZHENG QIAN*‡ and PINGWEN ZHANG†

†LMAM, CCSE and School of Mathematical Science, Peking University, Beijing 100871, China
‡Department of Mathematics, The Hong Kong University of Science and Technology, Clear Water Bay, Kowloon, Hong Kong, China

(*Received 12 December 2006; in final form 28 April 2007; accepted 1 June 2007*)

Using non-equilibrium molecular-dynamics (MD) simulations, we have measured the six Leslie coefficients of a nematic liquid crystal composed of molecules interacting via the Gay–Berne potential. In the presence of a simple shear flow, an alignment field is applied to control the molecular orientation and a uniform director is stabilized in the central region of the channel in which the liquid crystal is confined and sheared. With the director tuned by varying the applied field, a number of orientational states are stabilized in the presence of the shear flow and various viscous stress components are measured in these states of differently oriented directors. The six Leslie coefficients α_i are determined by interpreting the MD measurement data for viscous stress according to the constitutive relations in the Ericksen–Leslie–Parodi theory. Our measurement of the Leslie coefficients shows the Parodi relation $\alpha_2+\alpha_3=\alpha_6-\alpha_5$ is well satisfied. Given the values of the Leslie coefficients, liquid crystal orientations are evaluated for different alignment fields and shear rates, and then compared with those directly measured in MD simulations, demonstrating a quantitative agreement. Our simulation results show that in the Gay–Berne nematic liquid crystal, the viscous stress and the coupling between orientation and flow are well described by the Ericksen–Leslie–Parodi theory.

1. Introduction

Nematic liquid crystals (LCs) are liquids because they have no translational long-range order of molecules. However, they have long-range orientational order and therefore possess many special properties, from orientational elasticity to anisotropic viscosity. A continuum theory of elasticity has been developed by Oseen [1], Zocher [2] and Frank [3], followed by a theory of nematodynamics developed by Ericksen [4], Leslie [5] and Parodi [6]. In the Ericksen–Leslie–Parodi (ELP) theory, there are six viscosities called the Leslie coefficients with a constraint called the Parodi relation. The Leslie coefficients describe the anisotropic entropy production in LC flows and the interference of the dissipative processes associated with the translational and orientational degrees of freedom [7]. Theoretical modelling for the nematic LC viscosities has also been developed [8–13].

Molecular-dynamics (MD) simulations [14] have proved to be instrumental in the study of LC viscosities. Baalss and Hess [15] carried out non-equilibrium MD simulations for a perfectly ordered nematic LC composed of 'Lennard–Jones ellipsoids' with a fixed orientation (Maier–Saupe order parameter $s_2=1$) and measured the three Miesowicz viscosities [16] η_1, η_2 and η_3 and the two Leslie coefficients γ_1 and γ_2. Ehrentraut and Hess [17] then used the affine transformation model to study the viscosities for nematic LCs of imperfect order ($s<1$). Bennett *et al.* [18] studied the viscous behaviour of a perfectly ordered nematic LC composed of molecules of fixed orientation and interacting via the Gay–Berne potential [19], which is more realistic and has been widely used to model the intermolecular interaction for nematic LCs. Using the Gay–Berne potential, Bennettt and Hess [20] carried out non-equilibrium MD simulations to investigate the behaviour of the Miesowicz, Helfrich and Leslie viscosities as functions of density and temperature. According to the Green–Kubo theory of statistical physics, transport coefficients can be measured from various fluctuations in equilibrium. Sarman and Evans [21] derived the Green–Kubo relations for the viscosity coefficients of nematic LCs. Using the Gay–Berne potential, they carried out both equilibrium and non-equilibrium MD simulations, showing that the Green–Kubo results agree

*Corresponding author. Email: maqian@ust.hk

Liquid Crystals
ISSN 0267-8292 print/ISSN 1366-5855 online © 2007 Taylor & Francis
http://www.tandf.co.uk/journals
DOI: 10.1080/02678290701663878

well with those measured in non-equilibrium MD simulations. Sarman [22] then devised a Gaussian constraint algorithm that makes the angular velocity of the director a constant of motion. This algorithm can be used to fix the orientation of the director, necessitated by equilibrium MD simulations in small systems. Using the Gay–Berne potential, Smondyrev *et al.* [23] also carried out equilibrium MD simulations to measure the viscosities according to Kubo-like formulas and investigated their temperature dependence. With the director fixed by the constraint algorithm at different angles relative to the stream lines, Sarman [24] carried out non-equilibrium MD simulations of LC shear flow using the Gay–Berne potential, and measured the shear and rotational viscosities in a prolate nematic phase. Sarman [25] also calculated the Miesowicz viscosities of a variant of the Gay–Berne fluid as a function of temperature, first evaluated from the Green–Kubo relations in equilibrium and then cross-checked by performing shear flow simulations. Zakharov *et al.* [26] investigated the rotational viscosity coefficient and its relation with the rotational diffusion coefficient by a combination of statistical mechanical approaches and MD simulations. There is fairly extensive literature on the experimental measurements and studies of the LC viscosities. The complete set of the six Leslie coefficients of methoxybenzilidene butylanaline (MBBA) was reported by Kneppe *et al.* [27]. The Leslie coefficients of two high birefringence LC mixtures, E7 and UCF-2, were estimated based on the MBBA data by Wang *et al.* [28].

In this paper we carry out non-equilibrium MD simulations to measure the six Leslie coefficients α_i for a nematic LC modelled by the Gay–Berne intermolecular potential. In the presence of a simple shear flow, an alignment field is applied to control the LC director and various viscous stress components are measured in a series of selected orientational states with different directors. The Leslie coefficients are determined by interpreting the MD measurement data for viscous stress according to the constitutive relations in the ELP theory. Our measurement of the Leslie coefficients shows the Parodi relation $\alpha_2+\alpha_3=\alpha_6-\alpha_5$ is well satisfied. Given the values of the Leslie coefficients, a theoretical prediction of the LC orientation can be made in the presence of both the alignment field and shear flow, and a comparison with that directly measured in MD simulations exhibits quantitative agreement. Our simulation results show that in the Gay–Berne nematic LC, the viscous stress and the coupling between orientation and flow are well described by the ELP theory.

We want to point out that in measuring the LC viscosities, the present approach is similar to that in [20] in that a number of orientational states are stabilized by applying the alignment field and various viscous stress components are measured to determine the LC viscosities. In fact, in [20] there are six viscosities measured: three Miesowicz viscosities, one Helfrich viscosity and two Leslie (rotational) viscosities, which are equivalent to the six Leslie coefficients determined in the present work. Nevertheless, in [20] the stress measurement involves four orientational states only, three of which are for measuring the Miesowicz viscosities and Leslie (rotational) viscosities, and one of which is needed for measuring the Helfrich viscosity. In fact, in most of the earlier works only a few orientational states are used in determining various LC viscosities. In the present work, we use nearly 20 orientational states for determining one set of values for the six Leslie coefficients. By measuring the orientational dependence of various viscous stress components from many orientational states, we provide a direct verification of the continuum constitutive relations. It is through this verification that the values of the Leslie coefficients are determined. We want to point out that although our scheme for the measurement of the Leslie coefficients is presented using one special parametrization of the Gay–Berne potential, it can be applied to other parametrizations as well.

The paper is organized as follows. In section 2, we present the continuum theoretical considerations on how to determine the Leslie coefficients from the measurement of various viscous stress components in a set of selected orientational states and how to stabilize these orientational states by the application of alignment field. In section 3 we give the details of the MD simulations. In section 4 we present the numerical results for the Leslie coefficients and show the self-consistency of our results. The paper is concluded in section 5.

2. Theoretical considerations

In the ELP theory of the continuum nematodynamics [7], the viscous stress σ' in the regime of weak flow is expressed by

$$\begin{aligned}\sigma'_{\alpha\beta} &= \alpha_1 n_\alpha n_\beta n_\mu n_\nu A_{\mu\nu} + \alpha_4 A_{\alpha\beta} + \alpha_5 n_\alpha n_\mu A_{\mu\beta} \\ &\quad + \alpha_6 n_\beta n_\mu A_{\mu\alpha} + \alpha_2 n_\alpha N_\beta + \alpha_3 n_\beta N_\alpha,\end{aligned} \tag{1}$$

and the molecular field $\mathbf{h}$ is given by

$$h_\mu = \gamma_1 N_\mu + \gamma_2 n_\alpha A_{\mu\alpha}, \tag{2}$$

where the unit vector $\mathbf{n}$ is the director, $\mathbf{A}=1/2(\nabla\mathbf{v}+(\nabla\mathbf{v})^{\mathrm{T}})$ is the symmetric part of the velocity gradient tensor $\nabla\mathbf{v}$ and the vector $\mathbf{N}=\mathrm{d}\mathbf{n}/\mathrm{d}t-\boldsymbol{\omega}\times\mathbf{n}$ represents the rate of change of the director with respect to the background fluid, with $\boldsymbol{\omega}=\nabla\times\mathbf{v}/2$ being the antisymmetric part of the velocity gradient. The six Leslie coefficients α_i are linked by the Parodi relation $\alpha_2+\alpha_3=\alpha_6-\alpha_5$, and the coefficients

γ_1 and γ_2 are given by $\gamma_1=\alpha_3-\alpha_2$ and $\gamma_2=\alpha_2+\alpha_3$, respectively. To obtain the constitutive relations (1) and (2), each contribution to the entropy production is written as the product of a 'flux' and its conjugate 'force', and each force is expressed as a linear function of the fluxes (i.e. linear dissipative response).

To outline the scheme for the measurement of the Leslie coefficients, we consider a Couette flow of LCs with a uniform director $\mathbf{n}=(\cos\theta\cos\phi, \cos\theta\sin\phi, \sin\theta)$. The fluid velocity $\mathbf{v}$ is given by $v_x=\dot{\gamma}(z-H/2)$, $v_y=0$ and $v_z=0$, where $\dot{\gamma}=\partial v_x/\partial z$ is the shear rate and $H/2$ is the z coordinate of the midplane at which $v_x=0$. For special configurations of either $\phi=0$ or $\theta=0$, equation (1) can be further simplified. Below we call these configurations the XZ (with $\phi=0$) and XY (with $\theta=0$) configurations, respectively. For the XY configurations with $\mathbf{n}=(\cos\phi, \sin\phi, 0)$, we have

$$\sigma'_{xz}/\dot{\gamma}=\frac{1}{2}\alpha_4+\frac{1}{2}(\alpha_5+\alpha_2)\cos^2\phi, \tag{3}$$

$$\sigma'_{zx}/\dot{\gamma}=\frac{1}{2}\alpha_4+\frac{1}{2}(\alpha_6+\alpha_3)\cos^2\phi, \tag{4}$$

and for the XZ configurations with $\mathbf{n}=(\cos\theta, 0, \sin\theta)$, we have

$$\begin{aligned}\sigma'_{zx}/\dot{\gamma}&=\alpha_1\cos^2\theta\sin^2\theta+\frac{1}{2}(\alpha_6+\alpha_3)\cos^2\theta\\&+\frac{1}{2}(\alpha_5-\alpha_2)\sin^2\theta+\frac{1}{2}\alpha_4,\end{aligned} \tag{5}$$

$$\begin{aligned}\left(\sigma'_{xx}-\sigma'_{zz}\right)/\dot{\gamma}&=\alpha_1\left(\cos^3\theta\sin\theta-\sin^3\theta\cos\theta\right)\\&-(\alpha_2+\alpha_3)\cos\theta\sin\theta,\end{aligned} \tag{6}$$

$$\begin{aligned}\left(\sigma'_{zx}-\sigma'_{xz}\right)/\dot{\gamma}&=\frac{1}{2}(\alpha_6-\alpha_5)\left(\cos^2\theta-\sin^2\theta\right)\\&+\frac{1}{2}(\alpha_3-\alpha_2)\left(\cos^2\theta+\sin^2\theta\right).\end{aligned} \tag{7}$$

Our scheme for measuring the six Leslie coefficients in MD simulations may be described as follows.

(i) We stabilize, one by one, a series of the XY and XZ configurations of different directors.

(ii) We measure various viscous stress components and the shear rate in each steady configuration, obtaining those $\sigma'_{\alpha\beta}/\dot{\gamma}$ combinations needed in the left-hand side of equations (3)–(7).

(iii) We let the MD data collected for $\sigma'_{\alpha\beta}/\dot{\gamma}$ fit equations (4)–(7), using the ϕ and θ values measured directly in the steady states.

The values of the six α_i can be determined through this fitting procedure. While equation (3) is not needed in step (iii), which involves equations (4)–(7), it can still be used as an additional test of our measured results. We emphasize that the Parodi relation is not used in equation (1), from which equations (3)–(7) follow, in which all of the six coefficients are used. Therefore, it can be checked independently by the measured values of the Leslie coefficients. More details are presented in section 4.

The above fitting procedure needs a series of the XY and XZ configurations of different directors (i.e. different ϕ and θ values). To stabilize these orientational states in the presence of a Couette flow, an alignment field is applied to the system, with the interaction energy density given by $U_B=-b\left(\widehat{\mathbf{B}}\cdot\mathbf{n}\right)^2\Big/2$, where b measures the strength of the alignment and $\widehat{\mathbf{B}}$ is the unit vector in the direction of the field. Using the ELP theory, the relation between the applied field and the stabilized director can be derived.

In a system with a uniform director, there is no Frank–Oseen elastic free energy and the balance between the viscous molecular field and the molecular field $h_B=-\partial U_B/\partial n=b\left(\widehat{\mathbf{B}}\cdot\mathbf{n}\right)\widehat{\mathbf{B}}$ due to the applied field can be expressed as

$$\gamma_1\mathbf{N}+\gamma_2\mathbf{n}\cdot\mathbf{A}=\mathbf{h}_B+\lambda\mathbf{n}, \tag{8}$$

where λ is the Lagrange multiplier for $\mathbf{n}^2=1$.

According to equation (8), when the field is parallel to the xz plane, i.e. $\widehat{\boldsymbol{B}}=\left(\widehat{B}_x, 0, \widehat{B}_z\right)$, $\mathbf{n}=(\cos\theta, 0, \sin\theta)$ is a solution with θ determined by

$$P+Q\cos(2\theta)+R\sin(2\theta)=0, \tag{9}$$

where $P=-\gamma_1\dot{\gamma}$, $Q=2b\widehat{B}_x\widehat{B}_z-\gamma_2\dot{\gamma}$ and $R=b\left(\widehat{B}_z^2-\widehat{B}_x^2\right)$. If $\cos\theta=0$, then $2b\widehat{B}_x\widehat{B}_z=-(\gamma_1-\gamma_2)\dot{\gamma}$. Away from $\cos\theta=0$, equation (9) becomes

$$(P-Q)\tan^2\theta+2R\tan\theta+(P+Q)=0, \tag{10}$$

which is solvable because $\Delta=4R^2-4(P-Q)(P+Q)=4\left[b^2\left(\widehat{B}_x^2+\widehat{B}_z^2\right)^2-4b\widehat{B}_x\widehat{B}_z\gamma_2\dot{\gamma}+\left(\gamma_2^2-\gamma_1^2\right)\dot{\gamma}^2\right]>0$ with $\gamma_2<0$ and $|\gamma_2|>\gamma_1$ for rodlike nematic LCs.

To stabilize the XY configurations with $\mathbf{n}=(\cos\phi, \sin\phi, 0)$, $\widehat{\mathbf{B}}=\left(\widehat{B}_x, \widehat{B}_y, \widehat{B}_z\right)$ satisfies

$$\begin{aligned}&\left(\widehat{B}_x n_y-\widehat{B}_y n_x\right)\left(\widehat{\mathbf{B}}\cdot\mathbf{n}\right)=0,\\&2b\widehat{B}_y\widehat{B}_z\sin\phi=\left[(\gamma_1+\gamma_2)\dot{\gamma}-2b\widehat{B}_x\widehat{B}_z\right]\cos\phi.\end{aligned} \tag{11}$$

That is, $\widehat{B}_x=c\cos\phi$, $\widehat{B}_y=c\sin\phi$ and

$$\widehat{B}_z=\frac{(\gamma_1+\gamma_2)\dot{\gamma}\cos\phi}{2bc},$$

with c determined by $\widehat{\mathbf{B}}^2=1$. Here $B_y/B_x=\tan\phi$ indicates that the director is parallel to the projection of $\widehat{\mathbf{B}}$ on the xy plane. Physically, when $\gamma_2\neq-\gamma_1$, the flow-induced alignment in the absence of the applied field is away from the xy plane. Consequently, a non-zero $\widehat{B}_z$ is needed to stabilize $\mathbf{n}$ in the xy plane. This has been quantitatively verified in our simulations.

3. Molecular dynamics simulations

A nematic LC is confined by two planar solid walls parallel to the xy plane (see figure 1), with the fluid–solid boundaries defined by $z=0$ and H. Periodic boundary conditions are imposed in the x and y directions. The interaction between LC molecules is modelled by the Gay–Berne potential [19]

$$U_{\mathrm{GB}}(\mathbf{r},\hat{\mathbf{u}}_1,\hat{\mathbf{u}}_2)=4\epsilon(\hat{\mathbf{r}},\hat{\mathbf{u}}_1,\hat{\mathbf{u}}_2)\left[\left(\frac{\sigma_0}{r-\sigma(\hat{\mathbf{r}},\hat{\mathbf{u}}_1,\hat{\mathbf{u}}_2)+\sigma_0}\right)^{12}-\left(\frac{\sigma_0}{r-\sigma(\hat{\mathbf{r}},\hat{\mathbf{u}}_1,\hat{\mathbf{u}}_2)+\sigma_0}\right)^{6}\right], \quad (12)$$

where $\hat{\mathbf{u}}_1$ and $\hat{\mathbf{u}}_2$ are the unit vectors denoting the orientations of two interacting molecules separated by the position vector $\mathbf{r}=r\hat{\mathbf{r}}$, with $\hat{\mathbf{r}}$ being the unit vector. The energy and length parameters $\epsilon(\hat{\mathbf{r}},\hat{\mathbf{u}}_1,\hat{\mathbf{u}}_2)$ and $\sigma(\hat{\mathbf{r}},\hat{\mathbf{u}}_1,\hat{\mathbf{u}}_2)$ depend on the relative molecular orientation, giving the depth of the potential well and the intermolecular distance at which $U=0$, respectively. The length parameter is given by

$$\sigma(\hat{\mathbf{r}},\hat{\mathbf{u}}_1,\hat{\mathbf{u}}_2)=\sigma_0\left\{1-\frac{\chi}{2}\left[\frac{(\hat{\mathbf{r}}\cdot\hat{\mathbf{u}}_1+\hat{\mathbf{r}}\cdot\hat{\mathbf{u}}_2)^2}{1+\chi(\hat{\mathbf{u}}_1\cdot\hat{\mathbf{u}}_2)}+\frac{(\hat{\mathbf{r}}\cdot\hat{\mathbf{u}}_1-\hat{\mathbf{r}}\cdot\hat{\mathbf{u}}_2)^2}{1-\chi(\hat{\mathbf{u}}_1\cdot\hat{\mathbf{u}}_2)}\right]\right\}^{-1/2}, \quad (13)$$

where σ_0 is the length scale and χ is the parameter measuring the anisotropy of molecular shape: $\chi=[(\sigma_e/\sigma_s)^2-1]/[(\sigma_e/\sigma_s)^2+1]$, with σ_e and σ_s being the end-to-end and side-by-side separations of two anisotropic molecules, respectively. The energy parameter is given by

$$\epsilon(\hat{\mathbf{r}},\hat{\mathbf{u}}_1,\hat{\mathbf{u}}_2)=\epsilon_0[\epsilon(\hat{\mathbf{u}}_1,\hat{\mathbf{u}}_2)]^{\nu}[\epsilon'(\hat{\mathbf{r}},\hat{\mathbf{u}}_1,\hat{\mathbf{u}}_2)]^{\mu}, \quad (14)$$

where ϵ_0 is the energy scale,

$$\epsilon(\hat{\mathbf{u}}_1,\hat{\mathbf{u}}_2)=\left[1-\chi^2(\hat{\mathbf{u}}_1\cdot\hat{\mathbf{u}}_2)^2\right]^{-1/2} \quad (15)$$

and

$$\epsilon'(\hat{r},\hat{u}_1,\hat{u}_2)=1-\frac{\chi'}{2}\left[\frac{(\hat{\mathbf{r}}\cdot\hat{\mathbf{u}}_1+\hat{\mathbf{r}}\cdot\hat{\mathbf{u}}_2)^2}{1+\chi'(\hat{\mathbf{u}}_1\cdot\hat{\mathbf{u}}_2)}+\frac{(\hat{\mathbf{r}}\cdot\hat{\mathbf{u}}_1-\hat{\mathbf{r}}\cdot\hat{\mathbf{u}}_2)^2}{1-\chi'(\hat{\mathbf{u}}_1\cdot\hat{\mathbf{u}}_2)}\right]. \quad (16)$$

Here χ' is the parameter measuring the anisotropy of intermolecular interaction: $\chi'=[1-(\epsilon_e/\epsilon_s)^{1/\mu}]/[1+(\epsilon_e/\epsilon_s)^{1/\mu}]$, where ϵ_e/ϵ_s is the ratio of the well depths for end-to-end and side-by-side configurations.

The Gay–Berne potential needs four parameters (μ, ν, σ_e/σ_s, ϵ_e/ϵ_s). The interaction between LC molecules is modelled by $U_{\mathrm{ff}}=U_{\mathrm{GB}}^{(1,\,2,\,3,\,0.2)}$ (see [29]), with the energy and length scales given by $\epsilon_{\mathrm{ff}}=\epsilon_0$ and $\sigma_{\mathrm{ff}}=\sigma_0$. The wall molecules are modelled to be spherical and the interaction between a spherical wall molecule and an anisotropic LC molecule is modelled by an analogy to the Gay–Berne potential, $U_{\mathrm{wf}}=U_{\mathrm{GB}}(\mathbf{r},\mathbf{0},\hat{\mathbf{u}})$, where one of the two unit vectors in $U_{\mathrm{GB}}(\mathbf{r},\hat{\mathbf{u}}_1,\hat{\mathbf{u}}_2)$ is replaced by zero ($\hat{\mathbf{u}}_1\rightarrow\mathbf{0}$) for the spherical wall molecule while the other is kept ($\hat{\mathbf{u}}_2\rightarrow\hat{\mathbf{u}}$) to denote the orientation of the LC molecule. We use $\epsilon_{\mathrm{wf}}=2\epsilon_0$ and $\sigma_{\mathrm{wf}}=1.2\sigma_0$ as the energy scale and length scales for U_{wf}, in which the four parameters (μ, ν, σ_e/σ_s, ϵ_e/ϵ_s) are chosen to be (1, 2, $(3^{1/3}+3)/(3^{1/3}+1)$, 0.4) according to [30]. Throughout the remainder of this paper, all of the physical quantities are given in the MD reduced units defined in terms of ϵ_0, σ_0 and m.

To apply the alignment field, each LC molecule is put in an orientation-dependent potential $V_B=-b_0\left(\widehat{\mathbf{B}}\cdot\hat{\mathbf{u}}_i\right)^2/2$, where b_0 measures the coupling strength. Physically, this molecular parameter b_0 is proportional to the parameter b in the continuum field-induced energy density $U_B=-b\left(\widehat{\mathbf{B}}\cdot\mathbf{n}\right)^2/2$ used in section 2.

In our simulations, 6080 LC molecules are used for the XZ configurations and 6300 molecules for the XY configurations. The initial state of the LC is an fcc

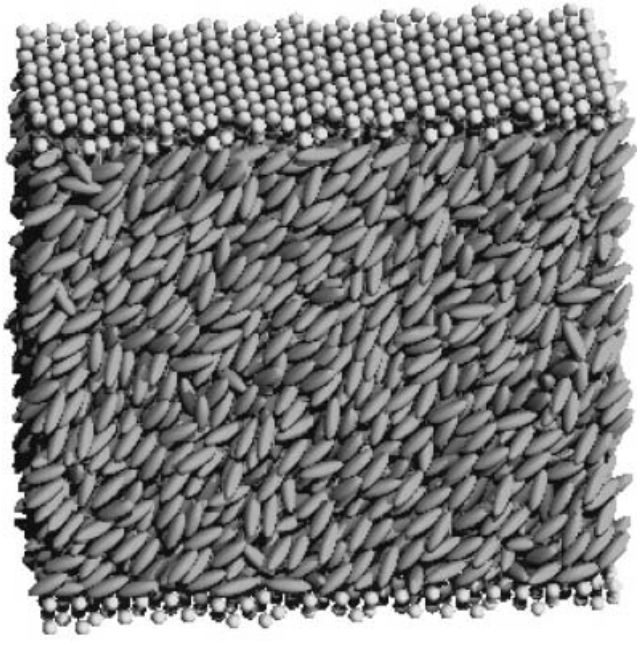

Figure 1. A snapshot of the molecular positions and orientations taken from one of our MD simulations. The spheres represent the wall molecules and the spheroids represent the LC molecules. The LC film is sheared by moving the two solid walls in opposite directions.

lattice with the number density $\rho_f = 0.3\sigma_0^{-3}$. The initial orientation of each LC molecule is $\hat{u}_i = (\cos 60^\circ, 0, \sin 60^\circ)$ in an XZ configuration or $\hat{u}_i = (\cos 45^\circ, \sin 45^\circ, 0)$ in an XY configuration. The moment of inertia is chosen to be $4m\sigma_0^2$. Each of the two walls is constructed by two [001] planes of an fcc lattice, with each wall molecule attached to the lattice site by a harmonic spring. The mean-squared displacement of the wall molecule is controlled to obey the Lindemann criterion. Each wall plane has 608 molecules with the number density $\rho_w = 0.4\sigma_0^{-3}$. The mass of the wall molecule is set equal to the mass of the LC molecule m. The potentials U_{ff} and U_{wf} are both truncated at $3.8\sigma_0$, and the equations of motion are integrated using a velocity Verlet algorithm with a time step $\Delta t = 0.001\sqrt{m\sigma_0^2/\epsilon_0}$. The translational and rotational temperatures of the LC are controlled using the Langevin noises and so is the temperature of the wall. These three temperatures are the same within statistical error in our simulations. Owing to the joint alignment effect of the applied field and shear flow, the temperature we use is $T = 2.5\epsilon_0/k_B$, which is a little bit higher than the nematic–isotropic phase transition point for $\rho_f = 0.3\sigma_0^{-3}$ in the absence of flow or field [29]. The Couette flow is generated by moving the top and bottom walls at a constant speed V_w in the $\pm x$ directions, respectively. Steady states are obtained for the XZ configurations with $H = 33.25\sigma_0$ and for the XY configurations with $H = 34.90\sigma_0$.

In order to measure the variations of various physical quantities in the z direction, the confined LC is divided into many layers. Each layer extends in the x and y directions and is of a small thickness $\Delta z \approx 1.5\sigma_0$ in the z direction. The shear rate $\dot{\gamma}$ is directly calculated from the velocity profile. The viscous stress components needed in our measurement of the Leslie coefficients are evaluated from the time averages of the kinetic momentum transfer rate and the intermolecular interaction contribution [15, 31]. The hydrostatic pressure can be obtained from the three diagonal components of the stress tensor. The (second-)order parameter s_2 is evaluated as a function of z from the largest eigenvalue of the tensorial order parameter

$$\mathbf{Q}(z) = \langle \sum_{i=1}^{N(z)} (3\hat{\mathbf{u}}_i\hat{\mathbf{u}}_i - \mathbf{I})/2N(z) \rangle,$$

where $N(z)$ is the number of particles in a particular layer [7]. The fourth order parameter s_4 is also measured from the time average of the fourth Legendre polynomial [32]. To focus on the central region of ideal Couette flow, which is characterized by uniform density, uniform director, uniform order parameters s_2 and s_4, constant shear rate and constant stress, we take arithmetical averages in the central fluid region, which is away from the confining walls by six bins ($\approx 9\sigma_0$), to obtain the fluid density ρ_f, the director $\hat{n}$, the order parameters s_2 and s_4, the shear rate $\dot{\gamma}$ and the stress components σ_{xx}, σ_{zz}, σ_{zx}, σ_{xz}. This avoids the undesired boundary effects due to the sliding boundaries used in our simulations. All of the quantities are measured by time averaging over 4×10^5 time steps following an initial relaxation of 5×10^5 time steps.

4. Results

We have carried out three sets of MD simulations using three different shear rates $2V_w/H = 0.066\sqrt{\epsilon_0/m\sigma_0^2}$, $0.044\sqrt{\epsilon_0/m\sigma_0^2}$ and $0.022\sqrt{\epsilon_0/m\sigma_0^2}$. (These shear rates are externally controlled by the simulation setup. The shear rates measured in the central Couette-flow region may be slightly different due to the boundary effects.) No slip is detected at the solid surface due to the small shear rates and the strong wall–fluid interaction. In each set of a particular shear rate, we have generated nine steady XZ configurations plus ten steady XY configurations. Each steady configuration displays a Couette flow (see figure 2) in the nematic phase, with the order parameter s_2 distributed around 0.75 (see figure 3) and the number density ρ_f around $0.295\sigma_0^{-3}$ (see figure 4) in the central region of the LC. Various stress components are measured in these states and all six Leslie coefficients are determined according to the fitting procedure described in section 2.

To tune the steady-state director in the Couette flow, we vary the field direction $\hat{\mathbf{B}}$, with the coupling constant

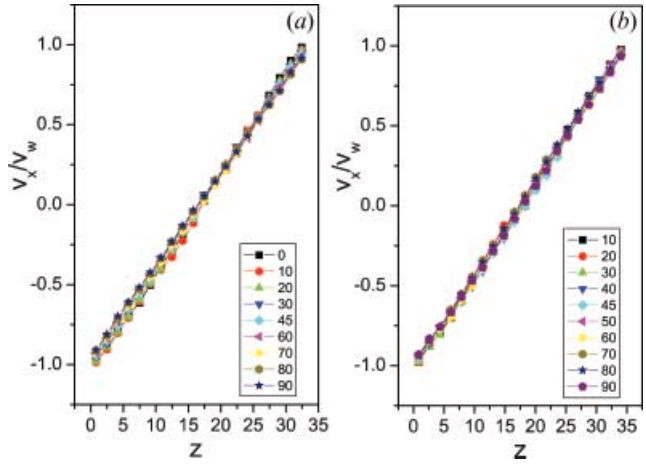

Figure 2. Scaled tangential velocity v_x/V_w plotted as a function of z: (a) in the XZ configurations, with the corresponding values of θ_B listed in the inset; (b) in the XY configurations, with the corresponding values of ϕ_B listed in the inset.

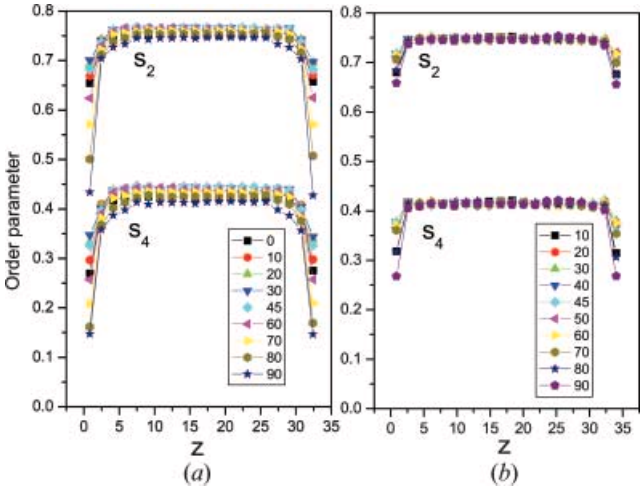

Figure 3. Local order parameters s_2 and s_4, each plotted as a function of z: (a) in the XZ configurations, with the corresponding values of θ_B listed in the inset; (b) in the XY configurations, with the corresponding values of ϕ_B listed in the inset. Note that the relation $s_4=s_2[1-(1-s_2)^{0.6}]$, proposed in [17], is satisfied here.

b_0 in V_B fixed at $6.25\epsilon_0$, which corresponds to the coupling constant $b=\rho_f s b_0=1.38\epsilon_0/\sigma_0^3$ in U_B. The relations between the applied field and the stabilized director in the shear flow are expressed by equations (9) and (11). To stabilize the XZ configurations, we use $\widehat{\mathbf{B}}=(\cos\theta_B, 0, \sin\theta_B)$ with θ_B=0°, 10°, 20°, 30°, 45°, 60°, 70°, 80° and 90°. Figure 5 (a) shows that in steady states, the average director is indeed parallel to the xz plane as its y component n_y is negligibly small. The tilt angle θ of $\mathbf{n}=(\cos\theta, 0, \sin\theta)$ is plotted as a function of z in figure 5 (b), showing a uniform director in the central region of the fluid.

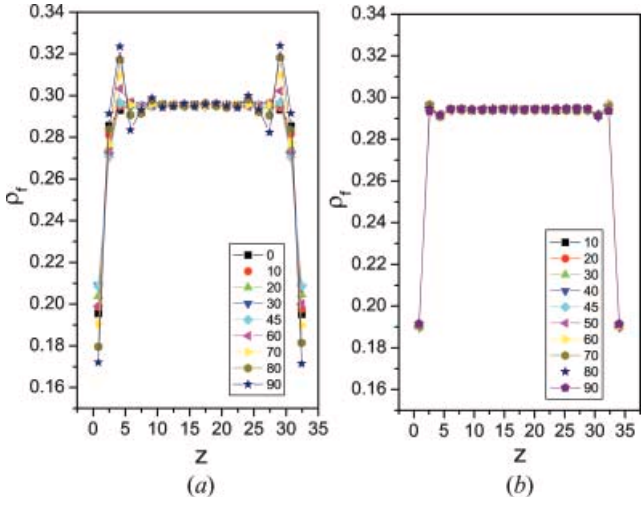

Figure 4. Local density ρ_f plotted as a function of z: (a) in the XZ configurations, with the corresponding values of θ_B listed in the inset; (b) in the XY configurations, with the corresponding values of ϕ_B listed in the inset.

To stabilize the XY configurations, we use $\widehat{\mathbf{B}}=c(\cos\phi_B, \sin\phi_B, a\cos\phi_B)$ (in which c is for normalization) with ϕ_B=10°, 20°, 30°, 40°, 45°, 50°, 60°, 70°, 80° and 90°. Here a is a small, negative parameter, approximately given by $(\gamma_1+\gamma_2)\dot{\gamma}/2b$. Before we have the values for γ_1 and γ_2, a is treated as an adjustable parameter, optimized to make the director parallel to the xy plane (see figure 5 (c)). The azimuthal angle ϕ of $\mathbf{n}=(\cos\phi, \sin\phi, 0)$ is plotted as a function of z in figure 5 (d), showing a uniform director in the central region. It is seen that the average azimuthal angle measured from the director in the central region agrees well with the azimuthal angle ϕ_B of the applied field, as predicted by equation (11).

The steady XZ and XY configurations all possess a central region of ideal Couette flow with uniform director, constant shear rate, and constant stress. In addition, in that region they have the same order parameters (s_2 and s_4), number density and temperature, and hence correspond to the same orientationally ordered state, for which we can determine the six Leslie coefficients from the measured viscous stress components according to the fitting procedure outlined in section 2 as follows.

(a) According to equation (4), the variation of $\sigma'_{zx}/\dot{\gamma}$ with ϕ in the XY configurations can be used to determine the values of α_4 and $\alpha_6+\alpha_3$ (see figure 6 (a)).

(b) According to equation (5), the variation of $\sigma'_{zx}/\dot{\gamma}$ with θ in the XZ configurations can be used to determine the values of α_1 and $\alpha_5-\alpha_2$ (see figure 6 (b)). Here the values of α_4 and $\alpha_6+\alpha_3$ determined in part (a) are needed.

(c) According to equation (6), the variation of $(\sigma'_{xx}-\sigma'_{zz})/\dot{\gamma}$ with θ in the XZ configurations can be used to determine the value of $\alpha_2+\alpha_3$ (see figure 6 (c)). Here the value of α_1 determined in part (b) is needed.

(d) According to equation (7), the variation of $(\sigma'_{zx}-\sigma'_{xz})/\dot{\gamma}$ with θ in the XZ configurations can be used to determine the value of $\alpha_3-\alpha_2$ (see figure 6 (d)). Here the value of $\alpha_6-\alpha_5$ is needed and it can be obtained from a linear combination of the values of $\alpha_6+\alpha_3$, $\alpha_5-\alpha_2$ and $\alpha_2+\alpha_3$ already determined in parts (a)–(c).

(e) With the six Leslie coefficients determined in (a)–(d), we use their values (listed in table 1) to evaluate $\sigma'_{xz}/\dot{\gamma}$ as a function of $n_x=\cos\phi$ in the XY configurations according to equation (3). The theoretical prediction so obtained can then be compared with the corresponding data directly

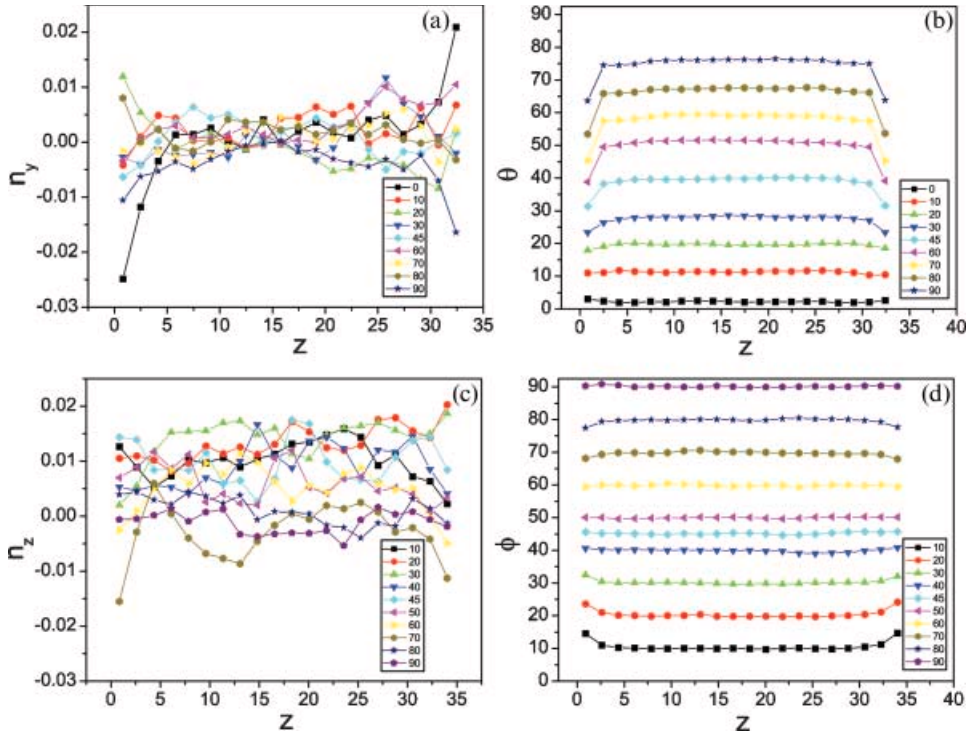

Figure 5. (a) The n_y component of the director plotted as a function of z in the XZ configurations. (b) The tilt angle θ of the director plotted as a function of z in the XZ configurations. In both (a) and (b), the corresponding values of θ_B are listed in the inset. (c) The n_z component of the director plotted as a function of z in the XY configurations. (d) The azimuthal angle ϕ of the director plotted as a function of z in the XY configurations. In both (c) and (d), the corresponding values of ϕ_B are listed in the inset.

measured in MD simulations, showing good agreement (see figure 7). Quantitatively, the range for the variation of $\sigma'_{xz}/\dot{\gamma}$ as a function of $n_x=\cos\phi$ is rather small, and hence the use of equation (3) is left to this last step, where the comparison for $\sigma'_{xz}/\dot{\gamma}$ in the XY configurations is mainly to show the self-consistency of our results.

(f) For the XZ configurations, the average tilt angle θ measured from the director in the central region can be compared with that predicted by equation (9) as soon as the values of $\gamma_1=\alpha_3-\alpha_2$ and $\gamma_2=\alpha_3+\alpha_2$ are determined. The agreement is very good (see figure 8), showing the self-consistency of our scheme again.

We note that the Parodi relation $\alpha_2+\alpha_3=\alpha_6-\alpha_5$ is well satisfied (see table 1). In addition, the signs of all of the six Leslie coefficients are in accordance with those measured for MBBA [27]. The three Miesowicz viscosities $\eta_1=(\alpha_3+\alpha_4+\alpha_6)/2$, $\eta_2=(-\alpha_2+\alpha_4+\alpha_5)/2$ and $\eta_3=\alpha_4/2$ are readily obtained from α_i. Ehrentraut and Hess [17] have formulated an affine transformation model for ellipsoidal particles with axis ratio Q, for both perfect and imperfect orders. They have shown that each of the three relative Miesowicz viscosities $\eta_1/\bar{\eta}$, $\eta_2/\bar{\eta}$ and $\eta_3/\bar{\eta}$, with $\bar{\eta}=(\eta_1+\eta_2+\eta_3)/3$, can be expressed in terms of Q and the order parameters s_2 and s_4. Substituting the values of these relative viscosities and the order parameters s_2 and s_4 into

$$\frac{\eta_2-\eta_1}{\eta}=\frac{s_2\left(Q^2-Q^{-2}\right)}{1+\frac{1}{15}(4+s_4)\left(Q-Q^{-1}\right)^2}$$

and

$$\frac{\eta_3}{\eta}=\frac{1-\frac{1}{15}\left(\frac{3}{7}s_4+\frac{25}{7}s_2-4\right)\left(Q-Q^{-1}\right)^2}{1+\frac{1}{15}(4+s_4)\left(Q-Q^{-1}\right)^2}$$

derived in [17], we can deduce the value of Q. This has been done using the values of $(\eta_2-\eta_1)/\bar{\eta}$ and $\eta_3/\bar{\eta}$ listed in table 1 and those of s_2 and s_4 displayed in figure 3. There is a total of three different values for $(\eta_2-\eta_1)/\bar{\eta}$ and two for $\eta_3/\bar{\eta}$, from which five different values of Q are deduced, ranging from 2.984 to 3.246. The fact that the values of Q so obtained are close to each other shows the self-consistency of our scheme and results. It is also interesting to note that these values of Q are very close to 3.0, the value of the parameter σ_e/σ_s in the Gay–Berne potential $U_{\mathrm{ff}}=U_{\mathrm{GB}}^{(1,\,2,\,3,\,0.2)}$ used in our simulations.

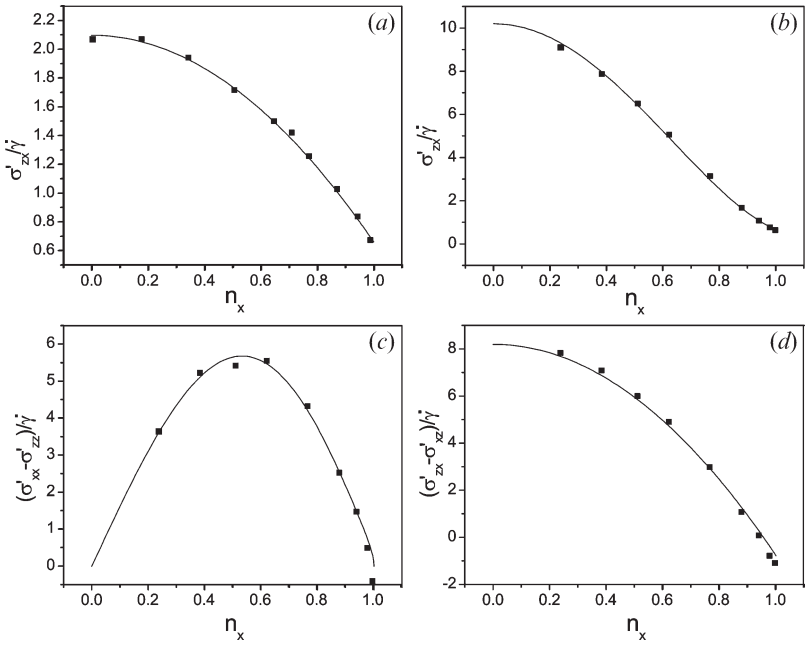

Figure 6. The fitting procedure in which the six Leslie coefficients are determined. The symbols denote the MD measurement data collected in nine XZ configurations and ten XY configurations of $2V_w/H=0.044\sqrt{\epsilon_0/m\sigma_0^2}$. The lines represent the theoretical predictions evaluated from equations (4), (5), (6) and (7), using the parameters listed in table 1 for $2V_w/H=0.044\sqrt{\epsilon_0/m\sigma_0^2}$. (a) $\sigma'_{zx}/\dot{\gamma}$ in the XY configurations, plotted as a function of $n_x=\cos\phi$. The solid curve represents $\sigma'_{zx}/\dot{\gamma}=\frac{1}{2}\alpha_4+\frac{1}{2}(\alpha_6+\alpha_3)\cos^2\phi=2.097-1.435\cos^2\phi$. (b) $\sigma'_{zx}/\dot{\gamma}$ in the XZ configurations, plotted as a function of $n_x=\cos\theta$. The solid curve represents $\sigma'_{zx}/\dot{\gamma}=\alpha_1\cos^2\theta\sin^2\theta+\frac{1}{2}(\alpha_6+\alpha_3)\cos^2\theta+\frac{1}{2}(\alpha_5-\alpha_2)\sin^2\theta+\frac{1}{2}\alpha_4=-6.716\cos^2\theta\sin^2\theta-1.435\cos^2\theta+8.099\sin^2\theta+2.097$. (c) $(\sigma'_{xx}-\sigma'_{zz})/\dot{\gamma}$ in the XZ configurations, plotted as a function of $n_x=\cos\theta$. The solid curve represents $(\sigma'_{xx}-\sigma'_{zz})/\dot{\gamma}=\alpha_1(\cos^3\theta\sin\theta-\sin^3\theta\cos\theta)-(\alpha_2+\alpha_3)\cos\theta\sin\theta=-6.716(\cos^3\theta\sin\theta-\sin^3\theta\cos\theta)+9.695\cos\theta\sin\theta$. (d) $(\sigma'_{zx}-\sigma'_{xz})/\dot{\gamma}$ in the XZ configurations, plotted as a function of $n_x=\cos\theta$. The solid curve represents $(\sigma'_{zx}-\sigma'_{xz})/\dot{\gamma}=\frac{1}{2}(\alpha_6-\alpha_5)(\cos^2\theta-\sin^2\theta)+\frac{1}{2}(\alpha_3-\alpha_2)(\cos^2\theta+\sin^2\theta)=-4.687(\cos^2\theta-\sin^2\theta)+3.710(\cos^2\theta+\sin^2\theta)$. Note that the $\dot{\gamma}$ used here is the shear rate measured in the central Couette-flow region, slightly different from the value of $2V_w/H$.

5. Concluding remarks

We have carried out non-equilibrium MD simulations of nematic LC flows. The six Leslie coefficients have been determined through the stress measurement in a set of orientational states. The validity of our results has been checked using the Parodi relation and also the LC orientation in the presence of both the alignment field and shear flow. To extract the hydrodynamic information out of the molecular motion, the shear rates $2V_w/H$ used in the simulations were fairly large. Consequently, to balance the strong flow alignment effect, a large

Table 1. The six Leslie coefficients determined from our non-equilibrium MD simulations of Couette flows with temperature $T=2.5\epsilon_0/k_B$, number density $\rho_f=0.295\sigma_0^{-3}$ and order parameter $s_2=0.75$ in the central region. The rotational viscosities γ_1 and γ_2 and the three relative Miesowicz viscosities $\eta_1/\bar{\eta}$, $\eta_2/\bar{\eta}$ and $\eta_3/\bar{\eta}$ are also listed, with $\gamma_1=\alpha_3-\alpha_2$, $\gamma_2=\alpha_3+\alpha_2$, $\eta_1=(\alpha_3+\alpha_4+\alpha_6)/2$, $\eta_2=(-\alpha_2+\alpha_4+\alpha_5)/2$, $\eta_3=\alpha_4/2$ and $\bar{\eta}=(\eta_1+\eta_2+\eta_3)/3$. The values of $(\alpha_2+\alpha_3)/(\alpha_6-\alpha_5)$ show that the Parodi relation $\alpha_2+\alpha_3=\alpha_6-\alpha_5$ is well satisfied.

$2V_w/H$	α_1	α_2	α_3	α_4	α_5	α_6
0.066	-5.98 ± 0.22	-8.59 ± 0.10	-1.09 ± 0.10	4.36 ± 0.03	7.60 ± 0.24	-2.00 ± 0.15
0.044	-6.72 ± 0.25	-8.56 ± 0.14	-1.14 ± 0.14	4.19 ± 0.02	7.64 ± 0.28	-1.73 ± 0.19
0.022	-6.88 ± 0.54	-8.56 ± 0.31	-1.11 ± 0.31	4.20 ± 0.04	7.14 ± 0.62	-1.68 ± 0.39

$2V_w/H$	γ_1	γ_2	$\eta_1/\bar{\eta}$	$\eta_2/\bar{\eta}$	$\eta_3/\bar{\eta}$	$(\alpha_2+\alpha_3)/(\alpha_6-\alpha_5)$
0.066	7.50	−9.67	0.15	2.35	0.50	1.01
0.044	7.42	−9.70	0.15	2.36	0.49	1.04
0.022	7.45	−9.67	0.17	2.34	0.49	1.10

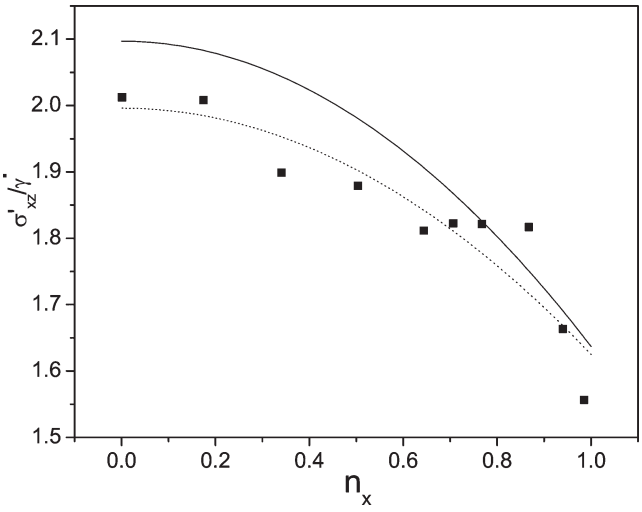

Figure 7. $\sigma'_{xz}/\dot{\gamma}$ in the XY configurations, plotted as a function of $n_x=\cos\phi$. The symbols denote the MD measurement data collected in ten XY configurations of $2V_w/H=0.044\sqrt{\epsilon_0/m\sigma_0^2}$. The solid curve represents $\sigma'_{zx}/\dot{\gamma}=\frac{1}{2}\alpha_4+\frac{1}{2}(\alpha_5+\alpha_2)\cos^2\phi=2.10-0.46\cos^2\phi$, using the parameters listed in table 1 for $2V_w/H=0.044\sqrt{\epsilon_0/m\sigma_0^2}$. Note that the relative difference between the symbols and the solid curve is larger than that in figure 6 because of the narrow range for the variation of $\sigma'_{xz}/\dot{\gamma}$ as a function of $n_x=\cos\phi$. The dotted curve represents $\sigma'_{xz}/\dot{\gamma}=2.00-0.37\cos^2\phi$ for the best fit.

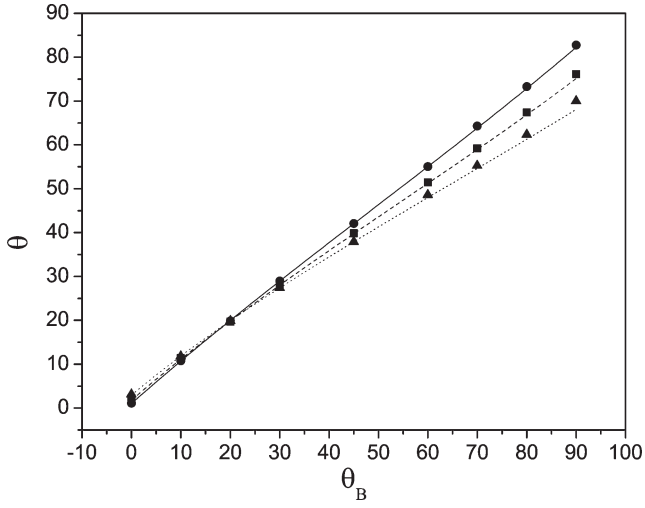

Figure 8. The director tilt angle θ plotted as a function of the field angle θ_B for the XZ configurations. The symbols denote the tilt angle measured from the director in the central region. The circles are for $2V_w/H=0.022\sqrt{\epsilon_0/m\sigma_0^2}$, the squares for $2V_w/H=0.044\sqrt{\epsilon_0/m\sigma_0^2}$ and the triangles for $2V_w/H=0.066\sqrt{\epsilon_0/m\sigma_0^2}$. The three curves are obtained from equation (9) using $b=1.38\epsilon_0/\sigma_0^3$, $\gamma_1=7.45\sqrt{\epsilon_0 m}/\sigma_0^2$ and $\gamma_2=-9.67\sqrt{\epsilon_0 m}/\sigma_0^2$ with $\dot{\gamma}=0.022\sqrt{\epsilon_0/m\sigma_0^2}$ (solid curve), $\gamma_1=7.42\sqrt{\epsilon_0 m}/\sigma_0^2$ and $\gamma_2=-9.70\sqrt{\epsilon_0 m}/\sigma_0^2$ with $\dot{\gamma}=0.044\sqrt{\epsilon_0/m\sigma_0^2}$ (dashed curve) or $\gamma_1=7.50\sqrt{\epsilon_0 m}/\sigma_0^2$ and $\gamma_2=-9.67\sqrt{\epsilon_0 m}/\sigma_0^2$ with $\dot{\gamma}=0.066\sqrt{\epsilon_0/m\sigma_0^2}$ (dotted curve). Note that each line passes through the point of $\theta=\theta_B=\frac{1}{2}\arccos(-\gamma_1/\gamma_2)$, which is the flow alignment angle, approximately 19.8° here.

coupling strength $b_0=6.25\epsilon_0$ has been used in the potential $V_B=-b_0\left(\hat{\mathbf{B}}\cdot\hat{\mathbf{u}}_i\right)^2\Big/2$ for field-induced alignment (along the unit vector $\hat{\boldsymbol{B}}$). This induces a fairly large nematic order parameter $s_2=0.75$ at $T=2.5\epsilon_0/k_B$, which is a little bit higher than the nematic–isotropic phase transition temperature [29]. We want to point out that although the shear rates and field strength used in the simulations are too large to be accessed in experiments, our scheme presented for determining the Leslie coefficients is still experimentally useful because of the following scaling relation. According to equation (9) and (11), if the shear rate $\dot{\gamma}$ scales with the field coupling strength b with $\dot{\gamma}/b$ kept constant, then the same set of the orientational states can be stabilized as well, but at much lower values of $\dot{\gamma}$ and b, thus accessible in experiments. In the limit of small field and small shear rate, the order parameter is only dependent on temperature and so are the viscosities.

Acknowledgements

Numerical computations were performed on a Beowulf cluster in the Center for Computational Science and Engineering of Peking University. T. Qian was partially supported by the Hong Kong RGC grant CA05/06.SC01. P. Zhang was partially supported by the special funds for Major State Research Projects 2005CB321704 and the National Science Foundation of China for Distinguished Young Scholars 10225103 and 20490222.

References

[1] C.W. Oseen. *Trans. Faraday Soc.*, **29**, 883 (1933).
[2] H. Zocher. *Trans. Faraday Soc.*, **29**, 945 (1933).
[3] F.C. Frank. *Discuss. Faraday Soc.*, **25**, 19 (1958).
[4] J.L. Ericksen. *Arch. Ration. Mech. Anal.*, **4**, 231 (1960).
[5] F.M. Leslie. *Arch. Ration. Mech. Anal.*, **28**, 265 (1968).
[6] O.J. Parodi. *J. Physique*, **31**, 581 (1970).
[7] P.G. de Gennes, J. Prost. *The Physics of Liquid Crystals*. Clarendon Press, Oxford (1993).
[8] H. Imura, K. Okano. *Jpn. J. Appl. Phys.*, **11**, 1440 (1972).
[9] A.C. Diogo, A.F. Martin. *Mol. Cryst. Liq. Cryst.*, **66**, 133 (1981).
[10] A.C. Diogo, A.F. Martin. *J. Physique*, **43**, 779 (1982).
[11] N. Kuzuu, M. Doi. *J. Phys. Soc. Jpn.*, **52**, 3486 (1983).
[12] N. Kuzuu, M. Doi. *J. Phys. Soc. Jpn.*, **53**, 1031 (1984).
[13] M.A. Osipov, E.M. Terentjev. *Phys. Lett. A*, **134**, 301 (1989).
[14] M.P. Allen, D.J. Tildesley. *Computer Simulation of Liquids*. Clarendon Press, New York (1987).

[15] D. Baalss, S. Hess. *Phys. Rev. Lett.*, **57**, 86 (1986).
[16] M. Miesowicz. *Nature*, **158**, 27 (1946).
[17] H. Ehrentraut, S. *Phys. Rev. E*, **51**, 2203 (1995).
[18] L. Bennett, S. Hess, C.P. Borgmeyer, T. Weider. *Int. J. Therm.*, **19**, 1143 (1998).
[19] J.G. Gay, B.J. Berne. *J. Chem. Phys.*, **74**, 3316 (1981).
[20] L. Bennett, S. Hess. *Phys. Rev. E*, **60**, 5561 (1999).
[21] S. Sarman, D.J. Evans. *J. Chem. Phys.*, **99**, 9021 (1993).
[22] S. Sarman. *J. Chem. Phys.*, **101**, 480 (1994).
[23] A.M. Smondyrev, G.B. Loriot, R.A. Pelcovits. *Phys. Rev. Lett.*, **75**, 2340 (1995).
[24] S. Sarman. *J. Chem. Phys.*, **103**, 10378 (1995).
[25] S. Sarman. *J. Chem. Phys.*, **108**, 7909 (1998).
[26] A.V. Zakharov, A.V. Komolkin, A. Maliniak. *Phys. Rev. E*, **59**, 6802 (1999).
[27] H. Kneppe, F. Schneider, N.K. Sharma. *J. Chem. Phys.*, **77**, 3203 (1982).
[28] H. Wang, T.X. Wu, S. Gauza, J.R. Wu, S.-T. Wu. *Liq. Cryst.*, **33**, 91 (2006).
[29] G.R. Luckhurst, R.A. Stephens. *Liq. Cryst.*, **8**, 451 (1990).
[30] T. Gruhn, M. Schoen. *Phys. Rev. E*, **55**, 2861 (1997).
[31] J.H. Irving, J.G. Kirkwood. *J. Chem. Phys.*, **18**, 817 (1950).
[32] P. Pasini, C. Zannoni. *Advances in the Computer Simulations of Liquid Crystals*, pp. pp. 17–50, Springer, Berlin (1999).